NeuroImage 226 (2021) 117591

Contents lists available at ScienceDirect

NeuroImage

journal homepage: www.elsevier.com/locate/neuroimage

# Relationship between the disrupted topological efficiency of the structural brain connectome and glucose hypometabolism in normal aging

Qiuhui Bi[a,b,1], Wenxiao Wang[a,b,1], Na Niu[c], He Li[a,b,d], Yezhou Wang[a,b], Weijie Huang[a,b], Kewei Chen[b,e], Kai Xu[a,b], Junying Zhang[a,b,d], Yaojing Chen[a,b], Dongfeng Wei[a,b,d], Ruixue Cui[c,**], Ni Shu[a,b,*], Zhanjun Zhang[a,b]

[a] State Key Laboratory of Cognitive Neuroscience and Learning & IDG/McGovern Institute for Brain Research, Beijing Normal University, Beijing 100875, PR China
[b] BABRI Centre, Beijing Normal University, Beijing 100875, PR China
[c] Department of Nuclear Medicine, Chinese Academy of Medical Sciences and Peking Union Medical College Hospital, Beijing 100730, PR China
[d] Institute of Basic Research in Clinical Medicine, China Academy of Traditional Chinese Medicine, Beijing 10070, PR China
[e] Banner Alzheimer's Institute, Phoenix, AZ 85006, USA

ARTICLE INFO

*Keywords:*
Brain network
Diffusion MRI
Graph theory
Glucose metabolism
FDG-PET
MRI
Normal aging

ABSTRACT

Normal aging is accompanied by structural degeneration and glucose hypometabolism in the human brain. However, the relationship between structural network disconnections and hypometabolism in normal aging remains largely unknown. In the present study, by combining MRI and PET techniques, we investigated the metabolic mechanism of the structural brain connectome and its relationship with normal aging in a cross-sectional, community-based cohort of 42 cognitively normal elderly individuals aged 57–84 years. The structural connectome was constructed based on diffusion MRI tractography, and the network efficiency metrics were quantified using graph theory analyses. FDG-PET scanning was performed to evaluate the glucose metabolic level in the cortical regions of the individuals. The results of this study demonstrated that both network efficiency and cortical metabolism decrease with age (both $p < 0.05$). In the subregions of the bilateral thalamus, significant correlations between nodal efficiency and cortical metabolism could be observed across subjects. Individual-level analyses indicated that brain regions with higher nodal efficiency tend to exhibit higher metabolic levels, implying a tight coupling between nodal efficiency and glucose metabolism ($r = 0.56$, $p = 1.15 \times 10^{-21}$). Moreover, efficiency-metabolism coupling coefficient significantly increased with age ($r = 0.44$, $p = 0.0046$). Finally, the main findings were also reproducible in the ADNI dataset. Together, our results demonstrate a close coupling between structural brain connectivity and cortical metabolism in normal elderly individuals and provide new insight that improve the present understanding of the metabolic mechanisms of structural brain disconnections in normal aging.

## 1. Introduction

Normal aging is accompanied by the degeneration of brain structures and functions, evident in such occurrences as gray matter atrophy, disruptions of white matter (WM) integrity and glucose hypometabolism. Advances in neuroimaging techniques, such as magnetic resonance imaging (MRI) and positron emission tomography (PET), allow researchers to investigate these dynamic brain changes with aging *in vivo*. With multimodal MRI techniques, numerous studies have reported structural and functional reorganization in elderly subjects. With PET, especially fluorodeoxyglucose PET (FDG-PET), the alterations in the underlying glucose metabolism in normal aging could be investigated directly.

The "disconnection aging" model has been proposed as a potential mechanism for cognitive aging (O'Sullivan et al., 2001). With the diffusion MRI technique, many researchers have observed a general trend of age-related diffusion changes in WM, especially in the frontal regions, indicating a deterioration in both the composition and integrity of WM (Bartzokis et al., 2012; Bennett and Madden, 2014; Kantarci et al., 2014; Lebel et al., 2012; Martensson et al., 2018; Stadlbauer et al., 2012). Similar results were also observed in longitudinal studies, demonstrating significant age-related alternations in WM integrity throughout the

* Corresponding author at: State Key Laboratory of Cognitive Neuroscience and Learning, Beijing Normal University, Beijing 100875, PR China.
** Corresponding author.
*E-mail addresses:* mmdhmm@126.com (R. Cui), nshu@bnu.edu.cn (N. Shu).
[1] These authors contributed to the work equally.

https://doi.org/10.1016/j.neuroimage.2020.117591
Received 10 August 2020; Received in revised form 2 November 2020; Accepted 19 November 2020
Available online 26 November 2020

brain (Barrick et al., 2010; Sullivan et al., 2010; Teipel et al., 2010). From the perspective of the brain connectome, the WM structural network can be mapped in *vivo* and exhibits many nontrivial topological properties, such as small-worldness, with both high global and local efficiency, suggesting an optimal balance of functional integration and segregation (Bullmore and Sporns, 2009; He and Evans, 2010). In normal aging, the structural brain connectome exhibits significant topological alterations, such as reduced network efficiency, loss of frontal hubs and increased modularity (Gong et al., 2009; Li et al., 2020; Wen et al., 2011; Zhao et al., 2015). Although WM changes during normal aging are nonpathological, they are likely to contribute to age-related cognitive decline in elderly subjects (Bender et al., 2016; Bennett et al., 2011; Madhavan et al., 2014; Sasson et al., 2013; Voineskos et al., 2012; Wolf et al., 2014; Yang et al., 2015).

In addition to the structural pathway, the generation and transmission of neural signals in the brain rely on the energy supply from the aerobic glycolysis of glucose. Therefore, neuronal death and a decrease in synaptic activity in healthy aging might result in a decrease in brain glucose metabolism in elderly individuals. In some lifespan studies, age-related decreases in glucose metabolism were observed in the frontal lobe, temporoparietal lobe and cingulate gyri (Castellano et al., 2019; Nugent et al., 2016). Moreover, several researchers have demonstrated the associations between WM degeneration and cortical hypometabolism during normal aging (Bartzokis et al., 2012; Chetelat et al., 2013; Cross et al., 2013; Inoue et al., 2008) and in subjects with cognitive impairment (Chetouani et al., 2018; Kuczynski et al., 2010; Schilling et al., 2019; Sintini et al., 2018). For example, metabolism in the frontal cortex is related to the fractional anisotropy values of the genu and splenium corpus callosum (Inoue et al., 2008), and frontal cortical hypometabolism is significantly associated with degeneration in long-range associative fibers (Chetelat et al., 2013). Together, these studies have suggested a link between WM degeneration and cortical glucose hypometabolism. However, most of the studies focused on the association between regional WM integrity and the metabolism of specific gray matter areas. The relationship between the ability of the structural brain network to transmit information and expend energy remains largely unclear.

Here, by combining diffusion MRI and FDG-PET techniques, we aimed to unravel the complicated relationship between structural connectivity degeneration and cortical hypometabolism in normal aging in a cross-sectional, community-based cohort of 42 cognitively normal elderly individuals aged 57–84 years. Based on diffusion MRI and tractography techniques, the topological efficiency metrics of the structural brain network were quantified and applied as a proxy of the integrity of whole-brain structural connectivity. Cerebral glucose metabolism was measured with FDG standard uptake value ratio (SUVr) values, which were computed from the FDG-PET image. First, we compared the age-related degeneration patterns of WM network efficiency and glucose metabolism. Then, we investigated the relationship between WM network efficiency and cortical metabolism during normal aging at global and regional levels. Finally, the reproducibility of the findings was validated with an alternative parcellation scheme and an independent dataset.

## 2. Materials and methods

### 2.1. Participants

*BABRI dataset.* Forty-two cognitively normal elderly participants were involved in the present study (age range 57–84 years, mean age 70.8 ± 7.1 years, 22 males); they were recruited from a large cohort included in the Beijing Aging Brain Rejuvenation Initiative (BABRI) project, an ongoing longitudinal study examining the brain and cognitive health in an elderly, community-dwelling sample. All of the participants were right-handed and native Chinese speakers. Participants were included in this study if they met the following criteria: 1) no history of addictions or neurologic, psychiatric, or systemic illnesses known to influence cognitive function, including head trauma, tumors, current depression, alcoholism, and epilepsy; 2) the ability to cope with the physical demands of an MRI procedure (no claustrophobia or Meniere's disease) and no metal in the body that did not meet the standard of MRI scans; 3) no suspected dementia or indication of an inability to complete the neuropsychological tests because of physical or mental disability; 4) no structural abnormalities other than cerebrovascular lesions, including tumors, subdural hematomas, and contusions due to previous head trauma that could impair cognitive function; 5) no large vessel diseases, such as cortical or subcortical infarcts and watershed infarcts; and 6) no diseases with WM lesions, such as multiple sclerosis. All of the participants were assessed for "clinical nondementia" status by using the DSM-IV, Petersen's MCI criteria (Petersen, 2004), and Clinical Dementia Rating score (CDR = 0), and all participants scored ≥ 24 on the Mini-Mental Status Examination (MMSE) (Zhang et al., 1990). This study followed the principles of the Declaration of Helsinki and was approved by the Institutional Review Board of the Beijing Normal University Imaging Center for Brain Research. Written informed consent was obtained from each participant.

*ADNI data set.* The validation dataset was from the Alzheimer's Disease Neuroimaging Initiative (ADNI) cohort. ADNI is a multisite longitudinal study (www.adni-info.org). The inclusion criteria of the participants in the present study were as follows: First, subjects diagnosed as cognitively healthy in the ADNI-2 cohort were included. Then, we selected individuals with available T1-weighted, DTI and FDG-PET images in the same follow-up. As we aimed to investigate the association between the WM structural network and brain metabolism, individuals were only included if the interval between DTI and FDG-PET scans was 3 months or less. Finally, forty cognitively normal participants with T1-weighted, DTI and FDG-PET images were included in this study (age range, 63–86 years; mean age 73.5 ± 5.5 years; 20 males). Detailed descriptions about the inclusion and exclusion criteria for the diagnostic groups can be found on the ADNI website (http://adni.loni.usc.edu/methods/).

### 2.2. Image acquisition

*BABRI data set.* MRI data were acquired with a Siemens Magnetom Trio 3T scanner at the Imaging Center for Brain Research, Beijing Normal University. Participants laid down still with their heads fixed in position by straps and foam to minimize movement. T1-weighted images were collected with sagittal 3D magnetization prepared rapid gradient echo (MP-RAGE) sequences, covering the entire brain (sagittal slices = 176, repetition time (TR) = 1900 ms, echo time (TE) = 3.44 ms, slice thickness = 1 mm, flip angle = 9°, inversion time = 900 ms, field of view (FOV) = 256 × 256 $mm^2$, and acquisition matrix = 256 × 256). DTI data were acquired using a single-shot, twice-focused, diffusion-weighted echo-planar imaging sequence (TR = 9500 ms, TE = 92 ms, 30 diffusion-weighted directions with a $b$ value of 1000 s/$mm^2$ and a single image with a $b$ value of 0 s/$mm^2$, axial slices = 70, slice thickness = 2 mm, no interslice gap, matrix size = 128 × 128, field of view = 256 × 256 $mm^2$, and voxel size = 2 × 2 × 2 $mm^3$). $^{18}$F-FDG scans were performed in Peking Union Medical College Hospital using a GE Discovery PET/CT Elite scanner (cortical thickness =3.75 mm, acquisition matrix = 192× 192). After a 30-min resting period, a bolus of 0.1 mCi/kg of FDG was injected at time 0. Then, data acquisition began 40–60 min after injection.

*ADNI dataset* . DTI and inversion-recovery spoiled gradient recalled (IR-SPGR) T1-weighted imaging data were acquired on several GE 3T scanners using scanner-specific protocols. Briefly, DTI data were acquired with a voxel size of 1.37 × 1.37 × 2.70 $mm^3$, 41 diffusion gradients with $b$ = 1000 s/$mm^2$ and 5 images with $b$ =0 s/$mm^2$. IR-SPGR data were acquired with a voxel size of 1.02 × 1.02 × 1.20 $mm^3$. FDG-PET imaging data were acquired on several types of scanners using different acquisition protocols. To increase data uniformity, the

data underwent a standardized preprocessing procedure during procedures for the ADNI project. Detailed descriptions of imaging protocols and preprocessing procedures are available at the ADNI website (http://adni.loni.usc.edu/methods/).

### 2.3. Image processing

*DTI data.* The preprocessing included eddy current and head motion correction, estimation of the diffusion tensor and calculation of the fractional anisotropy (FA). Briefly, the eddy current distortions and motion artifacts in the DTI data were corrected by applying an affine alignment of each DTI image to the b0 image. Accordingly, the b-matrix was reoriented based on the transformation matrix generated in eddy current correction. All preprocessing procedures of the DTI data were performed with the FDT toolbox in FSL (http://www.fmrib.ox.ac.uk/fsl). After preprocessing, the diffusion tensor was estimated by solving the Stejskal and Tanner equation. The FA of each voxel was calculated.

*FDG-PET data.* To quantify the FDG-SUVr, FDG-PET images were spatially normalized to the MNI space through T1-weighted images. Briefly, T1-weighted images were rigidly aligned to corresponding FDG-PET images. Then, the registered T1-weighted images were normalized to the MNI space, and this transformation was applied to the FDG-PET image. Global and regional SUVr were calculated by dividing the SUV of the whole brain and each ROI by the mean SUV of the cerebellum (Figure S1B). The ROIs were defined with the human Brainnetome Atlas with 246 brain regions (BNA-246) (210 cortical and 36 subcortical regions, Table S1) (Fan et al., 2016).

*ADNI dataset.* The original DTI, N3-corrected T1-weighted image and preprocessed FDG-PET data were downloaded from LONI (http://loni.usc.edu/). The details of data acquisition can be found at http://www.adni-info.org. The FDG-PET images were preprocessed by ADNI image preprocessing pipelines, including spatial alignment, averaging, and interpolation to a standard 2 mm isotropic voxel (detailed descriptions can be found at http://adni.loni.ucla.edu/methods/pet-analysis/preprocessing/). The procedures of DTI data processing and FDG-SUVr extraction were identical to the processing procedures of the BABRI dataset.

### 2.4. Brain network construction

The two fundamental elements of a network are nodes and edges. In this study, we constructed a WM structural network for each participant in both datasets using the following procedures.

*Network node definition.* The BNA-246 atlas (Fan et al., 2016) was used to define the network nodes. Briefly, the T1-weighted image of each subject was coregistered to the first b0 image in individual DTI space. The registered T1-weighted images were then nonlinearly transformed into the ICBM152 T1 template in MNI space. The inverse transformation was used to warp the BNA-246 atlas from MNI space into native DTI space. Discrete labeling values were preserved using a nearest-neighbor interpolation method. Using this procedure, we obtained 246 cortical and subcortical regions, each representing a node of the brain network (Figure S1A, Table S1). All procedures were performed using SPM12 software (http://www.fl.ion.ucl.ac.uk/spm/software/SPM12/).

*WM tractography.* DTI tractography was performed with the Diffusion Toolkit (https://www.trackvis.org/dtk/) with a deterministic tractography algorithm (Mori et al., 1999). All of the tracts in the dataset were computed by seeding each voxel with an FA that was greater than 0.2. Tractography was terminated if a tract turned at an angle greater than 45º or reached a voxel with an FA of less than 0.2. For each participant, tens of thousands of streamlines were generated to depict all of the major WM tracts.

*Network edge definition.* For the network edges, two regions were considered structurally connected if there was at least one fiber streamline with two endpoints that were located in these two regions. Specifically, we defined the number of interconnecting streamlines ending in two regions as the weights of the network edges. As a result, we constructed the fiber number (FN)-weighted WM network for each participant, which was represented by a symmetric 246 × 246 matrix (Fig. S1A).

### 2.5. Network analysis

*Global efficiency.* To characterize the topological organization of WM structural networks, the global efficiency of the whole brain network was assessed. The global efficiency of a graph G measures the efficiency of the parallel information transmission in the network (Latora and Marchiori, 2001) and can be calculated as follows:

$$E_{glob}(G) = \frac{1}{N(N-1)} \sum_{i \# j \in G} \frac{1}{L_{ij}}$$

where $L_{ij}$ is the shortest path length between node i and node j in graph G.

*Nodal efficiency.* To determine the nodal characteristics of the brain networks, we computed the nodal efficiency, $E_{nodal}$ (i), which is defined as (Achard and Bullmore, 2007)

$$E_{nodal}(i) = \frac{1}{N-1} \sum_{i \# j \in G} \frac{1}{L_{ij}}$$

where $L_{ij}$ is the shortest path length between node i and node j in G. The nodal efficiency measures the average shortest path length between a given node i and all of the other nodes in the network.

Graph theory analyses were performed using in-house GRETNA software (http://www.nitrc.org/projects/gretna/) (Wang et al., 2015), and the results were visualized using BrainNet Viewer software (http://www.nitrc.org/projects/bnv/) (Xia et al., 2013).

### 2.6. Statistical analyses

First, distributions of all continuous variables, including age and brain imaging measures, were tested for normality using the Kolmogorov–Smirnov test. Second, to identify the effects of age on the imaging measures, partial correlation analyses between age and brain imaging measures, such as network efficiency and FDG-SUVr at the global and regional levels, were performed across subjects. Sex and years of education were entered as covariates. For the regional analysis, the FDR correction for multiple comparisons was performed. Third, for the regions with significant age-related alterations, the relationship between cortical metabolism and nodal efficiency was also examined by partial correlation analysis while removing the effects of age, sex and years of education. Fourth, to examine the spatial coupling between cortical metabolism and network efficiency in elderly individuals, Pearson's correlation between regional nodal efficiency and FDG-SUVr metrics across regions was calculated both at individual and group averaged levels, resulting in a coupling coefficient for each subject. Finally, the correlation between the nodal efficiency-metabolism coupling coefficient and age was evaluated using Pearson's partial correlation, after removing the effects of sex and years of education. All of the statistical analyses were performed with MATLAB (R2018a).

### 2.7. Reproducibility analyses

To investigate the reproducibility of our results, we performed the following analyses to evaluate the effects of head motion, the effects of different parcellation schemes and the reproducibility from an independent dataset.

*Effects of head motion.* Although precautions were made to minimize involuntary head motion, the measures derived from diffusion-weighted imaging can still be influenced by head motion. To eliminate the effects of head movement, we evaluated the association between age and structural network efficiency and included sex, years of education and 4 averaged affine transformation parameters (translation, rotation, scaling and affine) estimated by FSL *eddy_correct* as covariates.

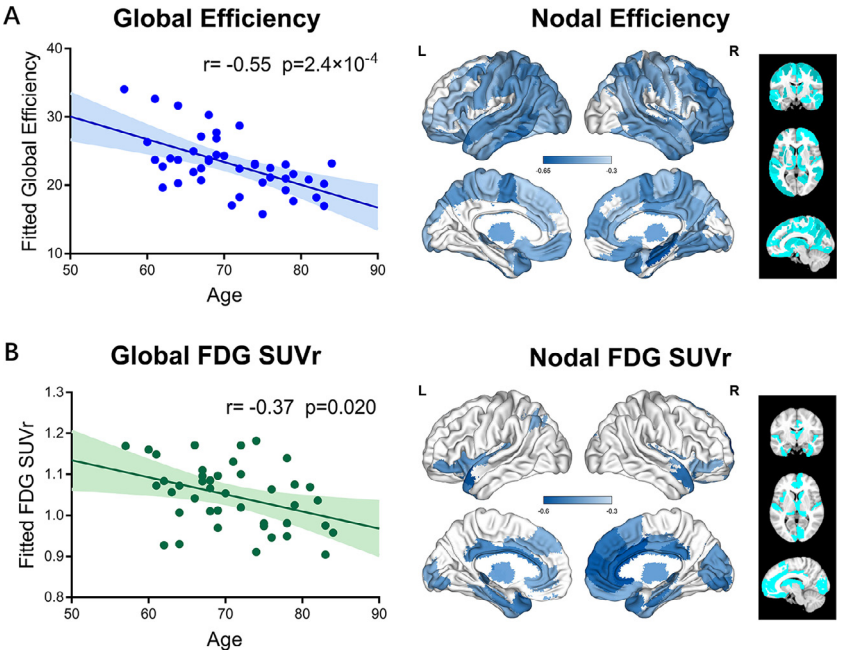


**Fig. 1.** The effects of age on network efficiency and cortical metabolism. (A) The global efficiency of the WM structural network showed significant decreases in normal aging (left). A 3D representation of brain regions with a significant age-related decline in nodal efficiency ($p < 0.05$, FDR corrected) (right). The color bar represents the value of the correlation coefficient ($r$ value) between age and nodal efficiency. (B) Whole-brain glucose metabolism (FDG-SUVr) showed significant decreases in normal aging (left). A 3D representation of brain regions with a significant age-related decline in glucose metabolism ($p < 0.05$, FDR corrected) (right). The color bar represents the value of the correlation coefficient ($r$ value) between age and regional FDG-SUVr values.

**Table 1**
Demographic characteristics of all participants.

| | BABRI ($n$ = 42) | ADNI ($n$ = 40) |
|---|---|---|
| Age (years) | 70.8 ± 7.1 (57–84) | 73.4 ± 5.5 (63–86) |
| Gender (M/F) | 22/20 | 20/20 |
| Education (years) | 11.6 ± 3.6 (3.5–17) | 16.4 ± 2.7 (12–20) |
| MMSE | 27.5 ± 2.1 (24–30) | 28.9 ± 1.3 (26–30) |

Data are presented as the mean±SD (range).
MMSE: Mini-mental State Examination.

*Effects of parcellation schemes.* Network efficiency metrics can be influenced by the definition of network nodes. To evaluate the effects of different brain parcellation schemes, we repeated the network construction with a contracted AAL atlas with 90 brain regions (AAL-90) according to Gong et al. (2008) (PANDA, https://www.nitrc.org/projects/panda/). Based on the AAL-90 network, similar network analyses were performed.

*Validation using the ADNI dataset.* Different MRI and PET scanning parameters used during data acquisition and different demographic characteristics of the research sample may also influence the reproducibility of the results. To evaluate the potential effects of these factors on the results, we repeated the network analysis procedures with the BAN-246 atlas with an independent dataset from the ADNI-2 cohort described above.

## 3. Results

### 3.1. Demographic information of all participants

The demographic characteristics of all participants are presented in Table 1. The BABRI dataset consisted of 42 healthy subjects (22 males) between the ages of 57 and 84 years (mean±std, 70.8 ± 7.1). These subjects completed 3.5–17 years of education (mean±std, 11.6 ± 3.6). A total of 40 subjects aged 63–86 years (mean±std, 73.4 ± 5.5) were included from the ADNI dataset (20 males). These subjects completed 12–20 years of education (mean±std, 16.4 ± 2.7). The distributions of age and years of education among groups are presented in Supplementary Fig. S2.

### 3.2. Age effects on WM network efficiency and glucose metabolism

Regarding the structural brain network, a significant age-related decline in network global efficiency was identified ($r$ = –0.55, $p = 2.4 \times 10^{-4}$) (Fig. 1A). Further analysis revealed that most of the brain regions demonstrated significant age-related decreases, especially in the right hippocampus, thalamus, frontal gyrus, including the middle frontal, orbital frontal (orbital and lateral areas), and superior frontal (dorsolateral and medial areas) areas; the left parietal gyrus, including the inferior parietal (rostro-dorsal area) and superior parietal (postcentral and rostral areas) areas; and the bilateral inferior and superior temporal areas, left precuneus and right cuneus ($p < 0.05$, FDR corrected) (Fig. 1A and Table S2).

For glucose metabolism, a significant age-related decline in whole-brain FDG-SUVr was also observed ($r$ = –0.37, $p$ = 0.020) (Fig. 1B). For regional alterations, we found that the FDG-SUVr values of the right anterior cingulate cortex, medial area of the right orbital and superior frontal gyrus, right occipital gyrus, caudal temporal thalamus, and bilateral lateral superior temporal gyrus exhibited significant decreases with age ($p < 0.05$, FDR corrected) (Fig. 1B and Table S3).

Specifically, some regions showed common decreases in both nodal efficiency and glucose metabolism; these areas were mainly located in the subregions of the bilateral thalamus, bilateral superior frontal gyrus, bilateral superior temporal gyrus, left insula, left angular gyrus, right cingulate gyrus, right orbital gyrus, right hippocampus, right striatum and right cuneus (Fig. 2). Further correlation analyses revealed that subregions of the thalamus (the rostral temporal thalamus, rTtha; occipital thalamus, Otha; and caudal temporal thalamus, cTtha) showed significantly positive correlations between nodal efficiency and cortical FDG-SUVr across subjects (rTtha. L: $r$ = 0.47, $p$ = 0.002; cTtha. L: $r$ = 0.59, $p = 7.3 \times 10^{-5}$; Otha. R: $r$ = 0.56, $p = 2.3 \times 10^{-4}$; cTtha. R: $r$ = 0.61, $p = 3.6 \times 10^{-5}$) (Fig. 2).

### 3.3. Spatial coupling between WM network efficiency and glucose metabolism

Similar spatial distributions of nodal efficiency and cortical metabolism are illustrated in Fig. 3. Specifically, regions with higher nodal efficiency were mainly distributed in the superior frontal gyrus,

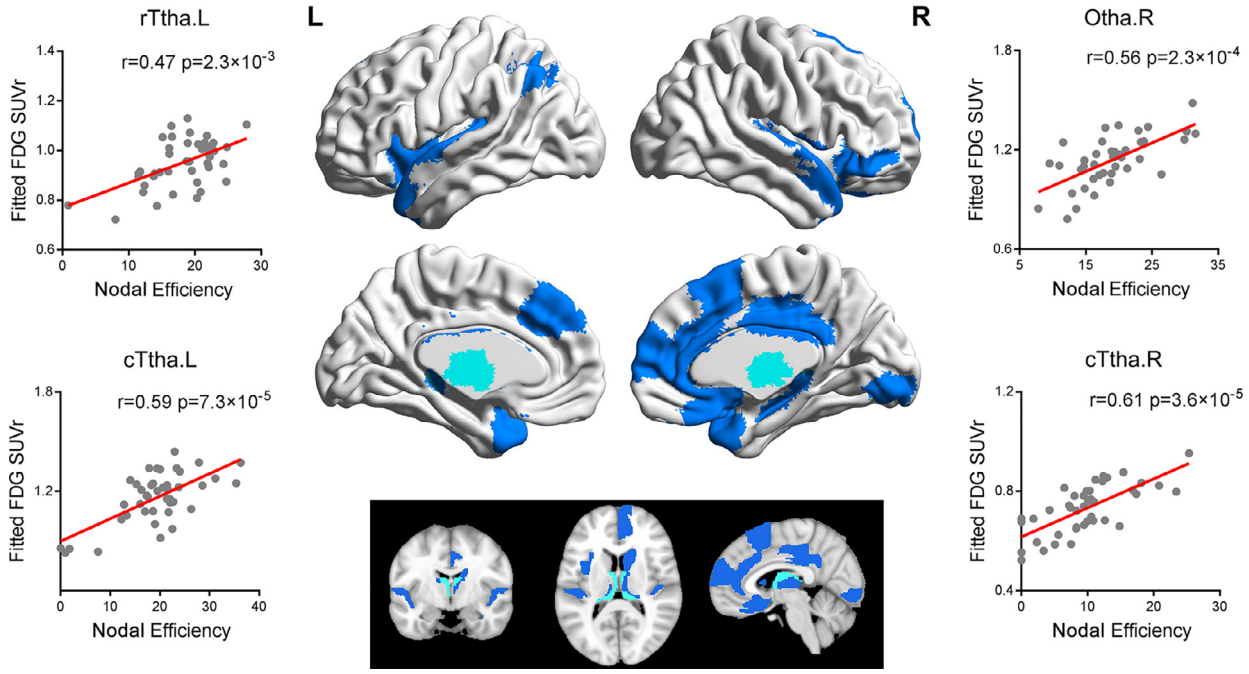


**Fig. 2.** The distribution of brain regions that showed common age-related decreases in both nodal efficiency and glucose metabolism. A 3D representation of brain regions with age-related decreases is shown in blue. Among these regions, the nodal efficiency of four thalamic subregions (cyan) was significantly correlated with their FDG-SUVr values across subjects. rTtha: rostral temporal thalamus; Otha: occipital thalamus; cTtha: caudal temporal thalamus.

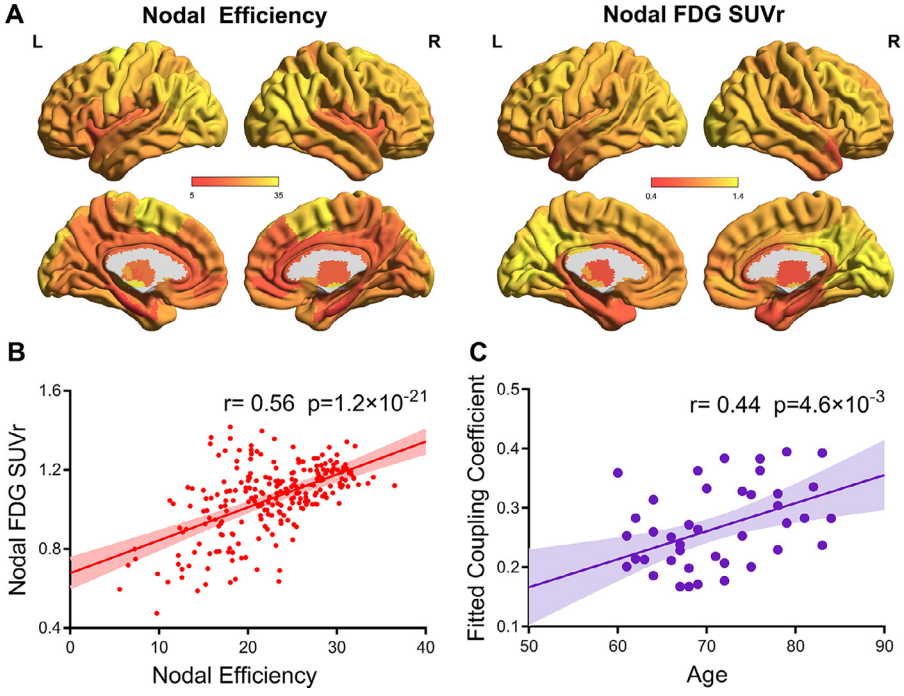


**Fig. 3.** The spatial distributions of group-averaged nodal efficiency and glucose metabolism. (A) Regional distributions of group-averaged nodal efficiency and regional FDG-SUVr. Brain regions with higher imaging measures are shown in yellow. (B) Significant correlation between group-averaged nodal efficiency and regional FDG-SUVr across regions. (C) Significant age effect on the coupling coefficient between nodal efficiency and FDG-SUVr.

angular gyrus, precentral gyrus, postcentral gyrus, middle frontal gyrus and occipital gyrus (Fig. 3A). For glucose metabolism, regions with higher FDG-SUVr values were mainly located in the cuneus, precuneus, occipital gyrus, precentral gyrus and middle frontal gyrus (Fig. 3A). Importantly, a significant correlation between regional nodal efficiency and regional FDG-SUVr across regions was found within each participant (coupling coefficient r from 0.24 to 0.58), as well as for the group average ($r$ = 0.56, $p$ = 1.2 × $10^{-21}$) (Fig. 3B), suggesting a strong coupling between nodal efficiency and cortical metabolism across regions at an individual level, implying that brain regions with higher nodal efficiency tend to consume more glucose metabolism.

As nodal efficiency and metabolism were spatially coupled with each other within individuals, we further examined how the coupling coefficient between these two measures would change with age. We found that the coupling coefficient significantly increased with age ($r$ = 0.44, $p = 4.6 \times 10^{-3}$) (Fig. 3C), suggesting a much stronger coupling between nodal efficiency and cortical metabolism in older subjects.

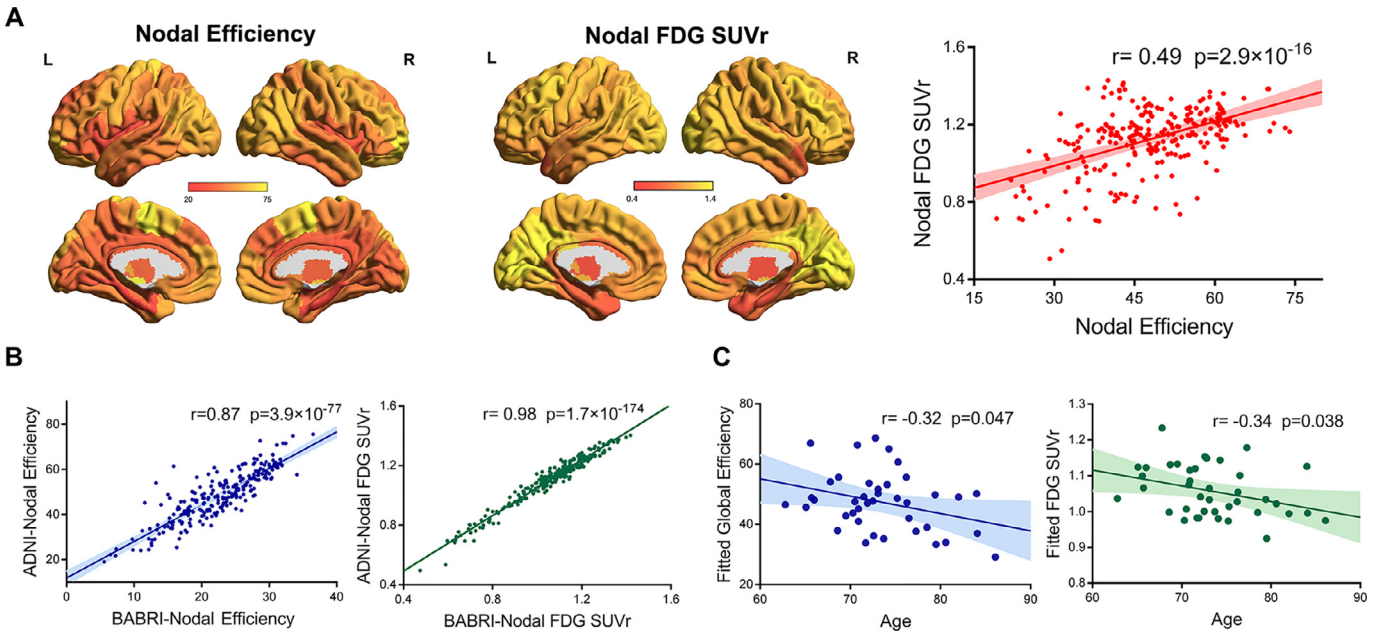


**Fig. 4.** Reproducibility of the findings using the ADNI dataset. (A) A 3D representation of the spatial distributions of nodal efficiency and glucose metabolism in the ADNI dataset. Strong coupling between nodal efficiency and cortical metabolism across regions was observed. (B) High correlation of nodal efficiency and FDG-SUVr values across regions between the BABRI and ADNI datasets was demonstrated. (C) Significant age effects were identified on whole-brain network global efficiency and glucose metabolism in the ADNI dataset.

### 3.4. Reproducibility of findings

*Effects of head motion.* The effects of age on brain network measures were evaluated with head motion parameters included as additional covariates. Similar effects of age were observed on network global efficiency ($r$ = -0.54, $p = 7.4 \times 10^{-4}$) (Fig. S3A) and nodal efficiency ($p < 0.05$, FDR corrected) (Fig. S3B).

*Validation using the AAL-90 atlas.* With AAL-90 parcellation for WM network construction, similar age effects were found on network global efficiency ($r$ = -0.44, $p = 4.5 \times 10^{-3}$) (Fig. S4A) and whole-brain FDG-SUVr ($r$ = -0.35, $p$ = 0.024) (Fig. S4B). Moreover, strong coupling between group-averaged nodal efficiency and cortical metabolism across regions was also observed ($r = 0.45$, $p = 6.7 \times 10^{-6}$) (Fig. S4C). Furthermore, a significant age-related increase was found in the coupling coefficient between nodal efficiency and nodal FDG-SUVr ($r = 0.33$, $p = 0.035$) (Fig. S4D).

*Validation using the ADNI dataset.* Despite the different demographic characteristics and scan parameters between the BABRI and ADNI datasets, highly similar spatial distributions of nodal efficiency ($r = 0.87$, $p = 3.9 \times 10^{-77}$) and nodal FDG-SUVr ($r = 0.98$, $p = 1.7 \times 10^{-174}$) were observed between these two datasets (Fig. 4B). Significant effects of age on both network global efficiency ($r$ = -0.32, $p = 0.047$) and whole-brain FDG–SUVr were also identified ($r$ = -0.34, $p$ = 0.038) (Fig. 4C). Moreover, tight coupling between group-averaged nodal efficiency and cortical metabolism across regions was found in the ADNI dataset ($r$ = 0.49, $p = 2.9 \times 10^{-16}$) (Fig. 4A). However, the age-related increase in the coupling coefficient could not be reproduced in the ADNI dataset ($p > 0.05$).

## 4. Discussion

In the present study, we examined the relationship between structural network efficiency and cortical glucose metabolism in normal aging in healthy elderly subjects by combining diffusion MRI and FDG-PET techniques. We confirmed that both WM structural network efficiency and glucose metabolism showed significant decreases in normal aging, which has been reported in previous studies. Furthermore, by combining these two imaging modalities, there are several novel findings from the perspective of the brain connectome. First, we observed a common decrease with significant correlations between nodal efficiency and glucose metabolism that was mainly located in the subregions of the bilateral thalamus. Second, the brain regions with higher nodal efficiency also exhibited higher glucose metabolism in elderly individuals, suggesting a strong spatial coupling between these two measures. Moreover, age-related increases in coupling coefficient was observed in elderly individuals. Overall, our results demonstrated a tight coupling between the structural network efficiency of the brain and cortical metabolism across regions in normal elderly subjects, which provided new insights for an improved understanding of the relationship between structural brain connectivity and glucose metabolism and that helps to unravel the potential metabolic mechanisms of structural brain disconnections that occur in normal aging.

### 4.1. Decreased brain network efficiency and metabolic level in normal aging

For the WM structural network, we observed a significant decline in global efficiency in normal aging, which is in accordance with the findings of previous studies (Ajilore et al., 2014; Fischer et al., 2014; Voineskos et al., 2012; Wen et al., 2011), implying a reorganized and less efficient structural brain network during a normal aging process. Regionally, the effects of age were most significant in the subregions of the right frontal regions and subcortical regions, including the thalamus and hippocampus. Similar results were also reported in previous studies, suggesting a selective age-related FA decline in anterior fibers (Bartzokis et al., 2012; Malykhin et al., 2011; O'Sullivan et al., 2001; Stadlbauer et al., 2012) as well as WM fibers connected to prefrontal regions (Sullivan et al., 2010).

With FDG-PET, we found decreased glucose metabolism in normal aging, mainly located in the right superior medial frontal gyrus, right anterior cingulate cortex and left superior temporal gyrus. These findings are consistent with many previous metabolic studies, which also reported decreased brain glucose uptake in elderly subjects, particularly in anterior regions, including the anterior cingulate and medial prefrontal cortex (Greve et al., 2016; Kalpouzos et al., 2009; Knopman et al.,

2014; Lebel et al., 2012; Pardo et al., 2007; Yoshizawa et al., 2014). As a biomarker of synaptic activity, the decrease in metabolism could be caused by the pruning of neural cells and cortical atrophy in the aging process.

Importantly, a common decrease between nodal efficiency and glucose metabolism was located in the subregions of the thalamus, where significant associations between these two imaging measures were further identified across subjects. In normal aging, disrupted WM integrity of the thalamus has been reported by many previous studies (Chetelat et al., 2013; Douet and Chang, 2014; Madden et al., 2012; Pelletier et al., 2013; Villain et al., 2008; Villain et al., 2010; Yang et al., 2016). As an important transition hub in the brain, the thalamus is involved in sensory input processing and is considered a principal route in interactions among cortical, subcortical, and brainstem nuclei. The majority of neurons in the thalamus represent relay cells, which contain triadic synapse complexes (Ralston, 1971). These relay cells receive thick fiber inputs from sensory relay nuclei and project to cerebral regions all over the brain, in which case synaptic activity might account for a crucial proportion of energy expenditure in the thalamus. Therefore, the metabolic level of the thalamus could be more sensitive to WM integrity alternation. From the perspective of the brain connectome, the disruption of this structural pathway would reduce the efficiency of information integration in the thalamus and therefore lead to a decrease in activity and hypometabolism in these regions (Kuczynski et al., 2010; Sintini et al., 2018).

### 4.2. Spatial coupling between brain network efficiency and glucose metabolism

The most important finding in the present study was that brain regions with higher nodal efficiency also tended to exhibit higher glucose metabolism, suggesting a strong coupling between network efficiency and metabolism within individuals. Previous studies combining rs-fMRI and FDG-PET techniques have demonstrated the high consistency between spatial distributions of glucose metabolic level and functional connectivity measures (Aiello et al., 2015; Li et al., 2013; Marchitelli et al., 2018; Tomasi et al., 2013). In particular, Liang et al. found that in the resting-state functional network of healthy adults, the distribution of network hubs largely overlapped with regions that had high regional cerebral blood flow (rCBF); also, rCBF was significantly correlated with functional network nodal centrality measures (Liang et al., 2013), suggesting that regions with higher functional connectivity strength tend to consume more energy. Although the association between brain structure and function was not consistently observed (Baum et al., 2020; Bennett and Rypma, 2013; Hagmann et al., 2008; Honey et al., 2009; Osmanlioglu et al., 2020; Preti and Van De Ville, 2019; Sui et al., 2014), the significant spatial coupling between structural network efficiency and glucose metabolism potentially implied that the capacity of information transmission of a region was related to its neural activities revealed by the metabolic level. Thus, DTI may provide unique information on metabolic changes in the brain during cognitive aging, which could not be explained by functional connectivity. In the future, multiple-modality studies combining DTI, fMRI and FDG-PET are needed to clarify the specific contributions to the hypometabolism in aging that are engendered by structural and functional changes in the brain.

Although the correlation between network efficiency and cerebral metabolism was found to be significant, a causal relationship could not be inferred in the current study. Previous DTI studies have investigated the relationship between local WM integrity and metabolism, indicating that the alteration of WM integrity would affect the metabolic level of the brain region to which it is attached (Bartzokis et al., 2012; Chetelat et al., 2013; Cross et al., 2013; Inoue et al., 2008). One theory is that glucose metabolism may affect the myelination of proximate or projecting tracts; another explanation is that the loss or degeneration of myelinated fibers decreases synaptic activity in surrounding or projecting cells (Bartzokis, 2004). In a longitudinal study by Villain et al., researchers found that hippocampal atrophy progressively led to the disruption of the cingulum bundle and uncinated fasciculus, and the reduction of information transmitted through the structural pathway finally led to hypometabolism in the cingulate and subgenual cortices. They also suggested that the influence of WM atrophy on remote metabolism was over and above that of local gray matter structural alterations (Villain et al., 2010). Thus, it is possible to hypothesize that reduced information transmission in network components with decreased network efficiency requires less energy and therefore leads to hypometabolism in related regions.

### 4.3. Increased nodal efficiency-metabolism coupling in normal aging

In addition to the age-related decline in network efficiency and metabolism, the coupling coefficient between these two measures was also significantly associated with age, exhibiting an increased efficiency-metabolism coupling in the aging process. Increased SC-FC coupling is usually observed in the developing brain, as white matter structural maturation, accompanied by synaptic plasticity and neurochemical modification, leading to a more integrated structural network and increased neural synchrony (Hagmann et al., 2010; Supekar et al., 2010; van den Heuvel and Fornito, 2014). However, Davis et al. found that under task conditions, regionwise SC-FC coupling may be stronger among older adults to prevent cognition decline by maintaining communication between regions (Davis et al., 2012). Similarly, a more recent study by Wang et al. indicated that the higher structural-functional coupling in cognitive impairment subjects was associated with poorer cognitive functions, suggesting that the disruption of the optimal structural organization may have given rise to SC-FC coupling alteration (Wang et al., 2018). In the current study, while the age-related decrement in nodal efficiency was widespread across the brain, the decrease in metabolism could be observed mostly in areas with lower nodal efficiency. In network hub regions such as the angular gyrus, precentral gyrus, postcentral gyrus, middle frontal gyrus and occipital gyrus, glucose metabolism remains relatively intact, which may also have contributed to higher efficiency-metabolism coupling. However, the increase in efficiency-metabolism coupling with age could not be reproduced in the validation analysis using the ADNI dataset, which may suggest that extra caution should be taken when interpreting this result.

### 4.4. Reproducibility analysis

Validation analyses were performed to evaluate the potential influence of network resolution and the generalizability of these findings in different populations. Significant age effects on global efficiency and cerebral metabolism, as well as the tight coupling between nodal efficiency and FDG-SUVr within individuals, were consistently observed using the AAL-90 atlas and in the ADNI dataset, implying the robustness of these results. However, the association between the efficiency-metabolism coupling coefficient and age could not be replicated in the ADNI dataset. This inconsistency may partly be due to the difference between the BABRI and ADNI groups. On average, individuals in the ADNI dataset completed more years of education than BABRI participants completed (Table 1). Although years of education are not associated with WM network efficiency or FDG-SUVr in the current study, the protective effect of education on brain structure and cognitive function in the aging process has been demonstrated in previous studies (Chen et al., 2019; Kim et al., 2015). Another possible explanation for the inconsistency could be the heterogeneity of data within the ADNI dataset. Although a standard protocol was performed in ADNI data collection to minimize the effect of multicenter imaging, the consistency and comparability of data from multiple centers and acquired using various scanners still need further evaluation.

### 4.5. Methodological issues

There are several strengths and limitations in this study. We used multimodal imaging data and connectome approaches to conduct comprehensive research on the relationship between WM network efficiency and metabolism in the normal aging process. The validation of alternative parcellation schemes and independent datasets avoided the bias induced by the network construction method and demographic characteristics, which might lead to center- or sample-specific findings. However, there were also some limitations in this study that should be noted. First, only structural network connections were included in the current study. Functional connections could exist between regions without a WM pathway. Thus, the portion of hypometabolism that could not be explained by WM alternations might be caused by functional changes. To develop a full picture of structural, functional and metabolic alterations in the brain in normal aging, a combined model with functional MRI evaluation should be developed in the future. Second, because cross-sectional data were implied, the causality between network efficiency and glucose metabolism could not be inferred from the current results. Further research should be undertaken to investigate the relationship between the WM network and glucose metabolism and their covariation in a longitudinal study design. Finally, although validation analyses were performed to examine the robustness of our results, the sample size was still small and might not provide a general representation of the healthy aging population. A larger sample would be beneficial to depict the linear or nonlinear correlation between age and imaging measures more precisely. In the future, we will continue to collect imaging data and validate the results with a larger sample.

## 5. Conclusions

By combining MRI and FDG-PET techniques, the present study demonstrated a tight coupling between structural brain connectivity and cortical metabolism across regions in normal elderly individuals, which may provide new insight that improve the present understanding of the relationship between structural brain connectivity and glucose metabolism and unravel the potential metabolic mechanisms of structural brain disconnections in normal aging.

## Financial Disclosures

There are no conflicts of interest including any financial, personal, or other relationships with people or organizations for any of the authors related to the work described in the article.

## Code availability

The MATLAB code for MRI and PET data processing is available from the authors upon request.

## Data for reference

The data sets generated and analyzed in the present study will be made available from the corresponding author to other scientists on request in anonymized format and according to data protection policy in the ethics agreement.

## Acknowledgments

The authors thank all the volunteers and patients for their participation in the study and anonymous reviewers for their insightful comments and suggestions.

This work was supported by the National Science Fund for Distinguished Young Scholars (grant number 81625025); Funds for International Cooperation and Exchange of the National Natural Science Foundation of China (grant number 81820108034); National Key Research and Development Project of China (grant number 2018YFC1315200); State Key Program of National Natural Science of China (grant number 81430100); National Natural Science Foundation of China (grant number 81471732, 81671761, 81871425, 81771874) and Fundamental Research Funds for the Central Universities (grant number 2017XTCX04).

## Supplementary materials

Supplementary material associated with this article can be found, in the online version, at doi:10.1016/j.neuroimage.2020.117591.

## References

Achard, S., Bullmore, E., 2007. Efficiency and cost of economical brain functional networks. PLOS Comput. Biol. 3, e17.

Aiello, M., Salvatore, E., Cachia, A., Pappata, S., Cavaliere, C., Prinster, A., Nicolai, E., Salvatore, M., Baron, J.C., Quarantelli, M., 2015. Relationship between simultaneously acquired resting-state regional cerebral glucose metabolism and functional MRI: a PET/MR hybrid scanner study. Neuroimage 113, 111–121.

Ajilore, O., Lamar, M., Kumar, A., 2014. Association of brain network efficiency with aging, depression, and cognition. Am. J. Geriatr. Psychiatry 22, 102–110.

Barrick, T.R., Charlton, R.A., Clark, C.A., Markus, H.S., 2010. White matter structural decline in normal ageing: a prospective longitudinal study using tract-based spatial statistics. Neuroimage 51, 565–577.

Bartzokis, G., 2004. Age-related myelin breakdown: a developmental model of cognitive decline and Alzheimer's disease. Neurobiol. Aging 25, 5–18.

Bartzokis, G., Lu, P.H., Heydari, P., Couvrette, A., Lee, G.J., Kalashyan, G., Freeman, F., Grinstead, J.W., Villablanca, P., Finn, J.P., Mintz, J., Alger, J.R., Altshuler, L.L., 2012. Multimodal magnetic resonance imaging assessment of white matter aging trajectories over the lifespan of healthy individuals. Biol. Psychiatry 72, 1026–1034.

Baum, G.L., Cui, Z., Roalf, D.R., Ciric, R., Betzel, R.F., Larsen, B., Cieslak, M., Cook, P.A., Xia, C.H., Moore, T.M., Ruparel, K., Oathes, D.J., Alexander-Bloch, A.F., Shinohara, R.T., Raznahan, A., Gur, R.E., Gur, R.C., Bassett, D.S., Satterthwaite, T.D., 2020. Development of structure-function coupling in human brain networks during youth. Proc. Natl. Acad. Sci. USA 117, 771–778.

Bender, A.R., Prindle, J.J., Brandmaier, A.M., Raz, N., 2016. White matter and memory in healthy adults: coupled changes over two years. Neuroimage 131, 193–204.

Bennett, I.J., Madden, D.J., 2014. Disconnected aging: cerebral white matter integrity and age-related differences in cognition. Neuroscience 276, 187–205.

Bennett, I.J., Madden, D.J., Vaidya, C.J., Howard Jr., J.H., Howard, D.V., 2011. White matter integrity correlates of implicit sequence learning in healthy aging. Neurobiol. Aging 32 (2317), e2311–e2312.

Bennett, I.J., Rypma, B., 2013. Advances in functional neuroanatomy: a review of combined DTI and fMRI studies in healthy younger and older adults. Neurosci. Biobehav. Rev. 37, 1201–1210.

Bullmore, E., Sporns, O., 2009. Complex brain networks: graph theoretical analysis of structural and functional systems. Nat. Rev. Neurosci. 10, 186–198.

Castellano, C.A., Hudon, C., Croteau, E., Fortier, M., St-Pierre, V., Vandenberghe, C., Nugent, S., Tremblay, S., Paquet, N., Lepage, M., Fulop, T., Turcotte, E.E., Dionne, I.J., Potvin, O., Duchesne, S., Cunnane, S.C., 2019. Links between metabolic and structural changes in the brain of cognitively normal older adults: a 4-year longitudinal follow-up. Front. Aging Neurosci. 11, 15.

Chen, Y., Lv, C., Li, X., Zhang, J., Chen, K., Liu, Z., Li, H., Fan, J., Qin, T., Luo, L., Zhang, Z., 2019. The positive impacts of early-life education on cognition, leisure activity, and brain structure in healthy aging. Aging 11, 4923–4942.

Chetelat, G., Landeau, B., Salmon, E., Yakushev, I., Bahri, M.A., Mezenge, F., Perrotin, A., Bastin, C., Manrique, A., Scheurich, A., Scheckenberger, M., Desgranges, B., Eustache, F., Fellgiebel, A., 2013. Relationships between brain metabolism decrease in normal aging and changes in structural and functional connectivity. Neuroimage 76, 167–177.

Chetouani, A., Chawki, M.B., Hossu, G., Kearney-Schwartz, A., Chauveau-Beuret, F., Bracard, S., Roch, V., Lebon, V., Marie, P.Y., Benetos, A., Joly, L., Verger, A., 2018. Cross–sectional variations of white and grey matter in older hypertensive patients with subjective memory complaints. Neuroimage Clin. 17, 804–810.

Cross, D.J., Anzai, Y., Petrie, E.C., Martin, N., Richards, T.L., Maravilla, K.R., Peskind, E.R., Minoshima, S., 2013. Loss of olfactory tract integrity affects cortical metabolism in the brain and olfactory regions in aging and mild cognitive impairment. J. Nucl. Med. 54, 1278–1284.

Davis, S.W., Kragel, J.E., Madden, D.J., Cabeza, R., 2012. The architecture of cross-hemispheric communication in the aging brain: linking behavior to functional and structural connectivity. Cereb. Cortex 22, 232–242.

Douet, V., Chang, L., 2014. Fornix as an imaging marker for episodic memory deficits in healthy aging and in various neurological disorders. Front. Aging Neurosci. 6, 343.

Fan, L., Li, H., Zhuo, J., Zhang, Y., Wang, J., Chen, L., Yang, Z., Chu, C., Xie, S., Laird, A.R., Fox, P.T., Eickhoff, S.B., Yu, C., Jiang, T., 2016. The human brainnetome atlas: a new brain atlas based on connectional architecture. Cereb. Cortex 26, 3508–3526.

Fischer, F.U., Wolf, D., Scheurich, A., Fellgiebel, A., 2014. Association of structural global brain network properties with intelligence in normal aging. PLoS One 9, e86258.

Gong, G., He, Y., Concha, L., Lebel, C., Gross, D.W., Evans, A.C., Beaulieu, C., 2008. Mapping anatomical connectivity patterns of human cerebral cortex using in vivo diffusion tensor imaging tractography. Cereb. Cortex 19, 524–536.

Gong, G., Rosa-Neto, P., Carbonell, F., Chen, Z.J., He, Y., Evans, A.C., 2009. Age- and gender-related differences in the cortical anatomical network. J. Neurosci. 29, 15684–15693.

Greve, D.N., Salat, D.H., Bowen, S.L., Izquierdo-Garcia, D., Schultz, A.P., Catana, C., Becker, J.A., Svarer, C., Knudsen, G.M., Sperling, R.A., Johnson, K.A., 2016. Different partial volume correction methods lead to different conclusions: an (18)F-FDG-PET study of aging. Neuroimage 132, 334–343.

Hagmann, P., Cammoun, L., Gigandet, X., Meuli, R., Honey, C.J., Wedeen, V.J., Sporns, O., 2008. Mapping the structural core of human cerebral cortex. PLoS Biol. 6, e159.

Hagmann, P., Sporns, O., Madan, N., Cammoun, L., Pienaar, R., Wedeen, V.J., Meuli, R., Thiran, J.P., Grant, P.E., 2010. White matter maturation reshapes structural connectivity in the late developing human brain. Proc. Natl. Acad. Sci. USA 107, 19067–19072.

He, Y., Evans, A., 2010. Graph theoretical modeling of brain connectivity. Curr. Opin. Neurol. 23, 341–350.

Honey, C.J., Sporns, O., Cammoun, L., Gigandet, X., Thiran, J.P., Meuli, R., Hagmann, P., 2009. Predicting human resting-state functional connectivity from structural connectivity. Proc. Natl. Acad. Sci. USA 106, 2035–2040.

Inoue, K., Ito, H., Uchida, S., Taki, Y., Kinomura, S., Tsuji, I., Sato, S., Horie, K., Kawashima, R., Ito, M., Fukuda, H., 2008. Decrease in glucose metabolism in frontal cortex associated with deterioration of microstructure of corpus callosum measured by diffusion tensor imaging in healthy elderly. Hum. Brain Mapp. 29, 375–384.

Kalpouzos, G., Chetelat, G., Baron, J.C., Landeau, B., Mevel, K., Godeau, C., Barre, L., Constans, J.M., Viader, F., Eustache, F., Desgranges, B., 2009. Voxel-based mapping of brain gray matter volume and glucose metabolism profiles in normal aging. Neurobiol. Aging 30, 112–124.

Kantarci, K., Schwarz, C.G., Reid, R.I., Przybelski, S.A., Lesnick, T.G., Zuk, S.M., Senjem, M.L., Gunter, J.L., Lowe, V., Machulda, M.M., Knopman, D.S., Petersen, R.C., Jack Jr., C.R., 2014. White matter integrity determined with diffusion tensor imaging in older adults without dementia: influence of amyloid load and neurodegeneration. JAMA Neurol. 71, 1547–1554.

Kim, J.P., Seo, S.W., Shin, H.Y., Ye, B.S., Yang, J.J., Kim, C., Kang, M., Jeon, S., Kim, H.J., Cho, H., Kim, J.H., Lee, J.M., Kim, S.T., Na, D.L., Guallar, E., 2015. Effects of education on aging-related cortical thinning among cognitively normal individuals. Neurology 85, 806–812.

Knopman, D.S., Jack Jr., C.R., Wiste, H.J., Lundt, E.S., Weigand, S.D., Vemuri, P., Lowe, V.J., Kantarci, K., Gunter, J.L., Senjem, M.L., Mielke, M.M., Roberts, R.O., Boeve, B.F., Petersen, R.C., 2014. 18F-fluorodeoxyglucose positron emission tomography, aging, and apolipoprotein E genotype in cognitively normal persons. Neurobiol. Aging 35, 2096–2106.

Kuczynski, B., Targan, E., Madison, C., Weiner, M., Zhang, Y., Reed, B., Chui, H.C., Jagust, W., 2010. White matter integrity and cortical metabolic associations in aging and dementia. Alzheimer's Dementia 6, 54–62.

Latora, V., Marchiori, M., 2001. Efficient behavior of small-world networks. Phys. Rev. Lett. 87, 198701.

Lebel, C., Gee, M., Camicioli, R., Wieler, M., Martin, W., Beaulieu, C., 2012. Diffusion tensor imaging of white matter tract evolution over the lifespan. Neuroimage 60, 340–352.

Li, X., Pu, F., Fan, Y., Niu, H., Li, S., Li, D., 2013. Age-related changes in brain structural covariance networks. Front. Hum. Neurosci. 7, 98.

Li, X., Wang, Y., Wang, W., Huang, W., Chen, K., Xu, K., Zhang, J., Chen, Y., Li, H., Wei, D., Shu, N., Zhang, Z., 2020. Age-related decline in the topological efficiency of the brain structural connectome and cognitive aging. Cereb. Cortex 30, 4651–4661.

Liang, X., Zou, Q., He, Y., Yang, Y., 2013. Coupling of functional connectivity and regional cerebral blood flow reveals a physiological basis for network hubs of the human brain. Proc. Natl. Acad. Sci. USA 110, 1929–1934.

Madden, D.J., Bennett, I.J., Burzynska, A., Potter, G.G., Chen, N.K., Song, A.W., 2012. Diffusion tensor imaging of cerebral white matter integrity in cognitive aging. Biochim. Biophys. Acta 1822, 386–400.

Madhavan, K.M., McQueeny, T., Howe, S.R., Shear, P., Szaflarski, J., 2014. Superior longitudinal fasciculus and language functioning in healthy aging. Brain Res. 1562, 11–22.

Malykhin, N., Vahidy, S., Michielse, S., Coupland, N., Camicioli, R., Seres, P., Carter, R., 2011. Structural organization of the prefrontal white matter pathways in the adult and aging brain measured by diffusion tensor imaging. Brain Struct. Funct. 216, 417–431.

Marchitelli, R., Aiello, M., Cachia, A., Quarantelli, M., Cavaliere, C., Postiglione, A., Tedeschi, G., Montella, P., Milan, G., Salvatore, M., Salvatore, E., Baron, J.C., Pappata, S., 2018. Simultaneous resting-state FDG-PET/fMRI in Alzheimer disease: relationship between glucose metabolism and intrinsic activity. Neuroimage 176, 246–258.

Martensson, J., Latt, J., Ahs, F., Fredrikson, M., Soderlund, H., Schioth, H.B., Kok, J., Kremer, B., van Westen, D., Larsson, E.M., Nilsson, M., 2018. Diffusion tensor imaging and tractography of the white matter in normal aging: the rate-of-change differs between segments within tracts. Magn. Reson. Imaging 45, 113–119.

Mori, S., Crain, B.J., Chacko, V.P., Van Zijl, P.C.M., 1999. Three-dimensional tracking of axonal projections in the brain by magnetic resonance imaging. Ann. Neurol. 45, 265–269.

Nugent, S., Castellano, C.A., Bocti, C., Dionne, I., Fulop, T., Cunnane, S.C., 2016. Relationship of metabolic and endocrine parameters to brain glucose metabolism in older adults: do cognitively-normal older adults have a particular metabolic phenotype? Biogerontology 17, 241–255.

O'Sullivan, M., Jones, D.K., Summers, P.E., Morris, R.G., Williams, S.C.R., Markus, H.S., 2001. Evidence for cortical "disconnection" as a mechanism of age-related cognitive decline. Neurology 57, 632–638.

Osmanlioglu, Y., Alappatt, J.A., Parker, D., Verma, R., 2020. Connectomic consistency: a systematic stability analysis of structural and functional connectivity. J. Neural Eng. 17, 045004.

Pardo, J.V., Lee, J.T., Sheikh, S.A., Surerus-Johnson, C., Shah, H., Munch, K.R., Carlis, J.V., Lewis, S.M., Kuskowski, M.A., Dysken, M.W., 2007. Where the brain grows old: decline in anterior cingulate and medial prefrontal function with normal aging. Neuroimage 35, 1231–1237.

Pelletier, A., Periot, O., Dilharreguy, B., Hiba, B., Bordessoules, M., Peres, K., Amieva, H., Dartigues, J.F., Allard, M., Catheline, G., 2013. Structural hippocampal network alterations during healthy aging: a multi-modal MRI study. Front. Aging Neurosci. 5, 84.

Petersen, R.C., 2004. Mild cognitive impairment as a diagnostic entity. J. Intern. Med. 256, 183–194.

Preti, M.G., Van De Ville, D., 2019. Decoupling of brain function from structure reveals regional behavioral specialization in humans. Nat. Commun. 10, 4747.

Ralston, H.J., 1971. Evidence for presynaptic dendrites and a proposal for their mechanism of action. Nature 230, 585–587.

Sasson, E., Doniger, G.M., Pasternak, O., Tarrasch, R., Assaf, Y., 2013. White matter correlates of cognitive domains in normal aging with diffusion tensor imaging. Front. Neurosci. 7, 32.

Schilling, L.P., Pascoal, T.A., Zimmer, E.R., Mathotaarachchi, S., Shin, M., de Mello Rieder, C.R., Gauthier, S., Palmini, A., Rosa-Neto, P., Alzheimer's Disease Neuroimaging, I., 2019. Regional amyloid-beta load and white matter abnormalities contribute to hypometabolism in Alzheimer's dementia. Mol. Neurobiol. 56, 4916–4924.

Sintini, I., Schwarz, C.G., Martin, P.R., Graff-Radford, J., Machulda, M.M., Senjem, M.L., Reid, R.I., Spychalla, A.J., Drubach, D.A., Lowe, V.J., Jack, C.R., Josephs, K.A., Whitwell, J.L., 2018. Regional multimodal relationships between tau, hypometabolism, atrophy, and fractional anisotropy in atypical Alzheimer's disease. Hum. Brain Mapp..

Stadlbauer, A., Ganslandt, O., Salomonowitz, E., Buchfelder, M., Hammen, T., Bachmair, J., Eberhardt, K., 2012. Magnetic resonance fiber density mapping of age-related white matter changes. Eur. J. Radiol. 81, 4005–4012.

Sui, J., Huster, R., Yu, Q., Segall, J.M., Calhoun, V.D., 2014. Function-structure associations of the brain: evidence from multimodal connectivity and covariance studies. Neuroimage 102 (Pt 1), 11–23.

Sullivan, E.V., Zahr, N.M., Rohlfing, T., Pfefferbaum, A., 2010. Fiber tracking functionally distinct components of the internal capsule. Neuropsychologia 48, 4155–4163.

Supekar, K., Uddin, L.Q., Prater, K., Amin, H., Greicius, M.D., Menon, V., 2010. Development of functional and structural connectivity within the default mode network in young children. Neuroimage 52, 290–301.

Teipel, S.J., Bokde, A.L., Meindl, T., Amaro Jr., E., Soldner, J., Reiser, M.F., Herpertz, S.C., Moller, H.J., Hampel, H., 2010. White matter microstructure underlying default mode network connectivity in the human brain. Neuroimage 49, 2021–2032.

Tomasi, D., Wang, G.J., Volkow, N.D., 2013. Energetic cost of brain functional connectivity. Proc. Natl. Acad. Sci. USA 110, 13642–13647.

van den Heuvel, M.P., Fornito, A., 2014. Brain networks in schizophrenia. Neuropsychol. Rev. 24, 32–48.

Villain, N., Desgranges, B., Viader, F., de la Sayette, V., Mezenge, F., Landeau, B., Baron, J.C., Eustache, F., Chetelat, G., 2008. Relationships between hippocampal atrophy, white matter disruption, and gray matter hypometabolism in Alzheimer's disease. J. Neurosci. 28, 6174–6181.

Villain, N., Fouquet, M., Baron, J.C., Mezenge, F., Landeau, B., de La Sayette, V., Viader, F., Eustache, F., Desgranges, B., Chetelat, G., 2010. Sequential relationships between grey matter and white matter atrophy and brain metabolic abnormalities in early Alzheimer's disease. Brain 133, 3301–3314.

Voineskos, A.N., Rajji, T.K., Lobaugh, N.J., Miranda, D., Shenton, M.E., Kennedy, J.L., Pollock, B.G., Mulsant, B.H., 2012. Age-related decline in white matter tract integrity and cognitive performance: a DTI tractography and structural equation modeling study. Neurobiol. Aging 33, 21–34.

Wang, J., Khosrowabadi, R., Ng, K.K., Hong, Z., Chong, J.S.X., Wang, Y., Chen, C.-Y., Hilal, S., Venketasubramanian, N., Wong, T.Y., Chen, C.L.-H., Ikram, M.K., Zhou, J., 2018. Alterations in brain network topology and structural-functional connectome coupling relate to cognitive impairment. Front. Aging Neurosci. 10.

Wang, J., Wang, X., Xia, M., Liao, X., Evans, A., He, Y., 2015. GRETNA: a graph theoretical network analysis toolbox for imaging connectomics. Front. Hum. Neurosci. 9, 386.

Wen, W., Zhu, W., He, Y., Kochan, N.A., Reppermund, S., Slavin, M.J., Brodaty, H., Crawford, J., Xia, A., Sachdev, P., 2011. Discrete neuroanatomical networks are associated with specific cognitive abilities in old age. J. Neurosci. 31, 1204–1212.

Wolf, D., Fischer, F.U., Fesenbeckh, J., Yakushev, I., Lelieveld, I.M., Scheurich, A., Schermuly, I., Zschutschke, L., Fellgiebel, A., 2014. Structural integrity of the corpus callosum predicts long-term transfer of fluid intelligence-related training gains in normal aging. Hum. Brain Mapp. 35, 309–318.

Xia, M., Wang, J., He, Y., 2013. BrainNet viewer: a network visualization tool for human brain connectomics. PLoS One 8, e68910.

Yang, A.C., Tsai, S.J., Liu, M.E., Huang, C.C., Lin, C.P., 2016. The association of aging with white matter integrity and functional connectivity hubs. Front. Aging Neurosci. 8, 143.

Yang, Y., Bender, A.R., Raz, N., 2015. Age related differences in reaction time components and diffusion properties of normal-appearing white matter in healthy adults. Neuropsychologia 66, 246–258.

Yoshizawa, H., Gazes, Y., Stern, Y., Miyata, Y., Uchiyama, S., 2014. Characterizing the normative profile of 18F-FDG PET brain imaging: sex difference, aging effect, and cognitive reserve. Psychiatry Res. 221, 78–85.

Zhang, M., Katzman, R., Salmon, D., Jin, H., Cai, G., Wang, Z., Qu, G., Grant, I., Yu, E., Levy, P., Klauber, M.R., Liu, W.T., 1990. The prevalence of dementia and Alzheimer's disease in Shanghai, China: impact of age, gender, and education. Ann. Neurol. 27, 428–437.

Zhao, T., Cao, M., Niu, H., Zuo, X.N., Evans, A., He, Y., Dong, Q., Shu, N., 2015. Age-related changes in the topological organization of the white matter structural connectome across the human lifespan. Hum. Brain Mapp. 36, 3777–3792.